Effective Midrange Wireless Power Transfer with Compensated Radiation Loss

N. Ha-Van,* C.R. Simovski, F.S. Cuesta, P. Jayathurathnage, and S.A. Tretyakov
Department of Electronics and Nanoengineering, Aalto University, P.O. Box 15500, Aalto FI-00076, Finland

(Received 3 February 2023; revised 11 April 2023; accepted 26 June 2023; published 20 July 2023)

In conventional inductive wireless power devices, the energy is transferred via only reactive near fields, which is equivalent to nonradiative Förster energy transfer in optics. Radiation from transmitting and receiving coils is usually considered as a parasitic effect that reduces the power-transfer efficiency. As long as the distance between the two antennas is small compared to the antenna size, conventional wireless power-transfer devices offer rather high power-transfer efficiency, of the order of 80%–90%. However, for larger distances, the transfer efficiency dramatically drops, making such devices impractical. In this paper, we develop a dynamic theory of wireless power transfer between two small loop antennas, clarify the role of far-field radiation, and find a possibility to realize efficient wireless power transfer at large distances utilizing the regime of radiation suppression due to optimized mutual dynamic interactions between the transmitting and receiving antennas. The analytical results are validated by simulations and measurements, and they open a possibility to greatly expand the range of distances of compact wireless power-transfer devices. The developed theory can also be applied to coupling between antennas of different types and to energy transfer between nano-objects.

DOI: 10.1103/PhysRevApplied.20.014044

I. INTRODUCTION

Wireless power-transfer (WPT) technologies have become more and more important for many diverse applications, such as charging of mobile telecommunication devices, electric vehicles, implantable medical devices, robots, wearable electronics, and in energy harvesting systems (see, e.g., Refs. [1–3]). In recent decades, the proliferation of wireless devices has especially motivated fast developments of wireless powering and charging technologies.

All WPT systems can be classified into near-field and far-field ones (see, e.g., Ref. [4]). When the distance between the transmitting and receiving antennas is small compared to the wavelength, the reactive near fields at the receiver position are much stronger than slower decaying fields of propagating waves created by the transmitting antenna. In this short-range WPT regime, the power is transferred predominantly by the near fields, whereas the radiation is usually considered as a parasitic factor resulting in some radiation loss that decreases efficiency (see, e.g., Refs. [5–12]). In this regime it appears that it is desirable to suppress antenna radiation. However, the radiative fields are also present in the near zone and they may contribute to the received power.

If the distance between the transmitting and receiving antennas is electrically large, the near fields of the transmitting antenna become negligibly small compared to the radiation fields. For electrically small and weakly directive antennas, the transfer efficiency becomes very small. For this reason, in long-range radiative WPT systems high-directivity antennas are used in both receiving (RX) and transmitting (TX) devices. Obviously, in this case, radiation is used as the main power-transfer mechanism, and radiation losses can be reduced only by using higher-gain antennas of large sizes in comparison with the wavelength.

In this paper, we consider the intermediate case of midrange wireless power transfer, where at the receiver position near fields of the transmitter significantly decay and the slower-decaying radiative fields become comparably strong or even stronger. Specifically, we define the midrange regime in terms of the electromagnetic distance kd between the two antennas. In the magnetic dipole regime of a loop antenna, the radius of the loop a is restricted so that $a < \lambda/6\pi$. Taking this condition into account we define the midrange as $0.2\pi \leq kd \leq 2\pi$. In this situation, radiation of energy into the far zone is still unwanted, as this is one of the loss mechanisms. On the other hand, radiative fields can significantly contribute to the power transfer to the receiving antenna. In practice, this situation corresponds to scenarios where the distance between the transmitting and receiving antennas is large compared to the sizes of the antennas, while the antennas themselves are electrically small. Realization of such WPT systems would allow wireless power transfer using compact devices, as the transfer distance can be large compared to both connected devices. It is expected that the

*nam.havan@aalto.fi

power-transfer efficiency, in this case, will be lower than for near-field coupling devices working at small transfer distances, but it may be possible to also realize reasonable efficiency at large separations by exploiting coupling by both near fields and radiative fields.

In this study, we develop the dynamic theory of wireless power transfer between two magnetic dipole antennas and use it to study the role of radiation fields (intermediate and far zone) in the transfer of power. In all works on electromagnetic coupling between two antennas, one distinguishes the quasistatic model that neglects the radiative coupling and takes into account only the term $1/r^3$ in the Green function. Whereas the dynamic model is based on the exact Green function, also incorporating the intermediate- and near-field term $1/r^2$ and the far-field term $1/r$. By taking these factors into account, the dynamic theory offers a comprehensive analysis of the electromagnetic coupling between two antennas and clarifies the role of radiation in power transfer. We answer the following questions. What is the dominant role of dynamic (far-zone) fields—disadvantage of parasitic radiation loss or an advantage of higher electromotive force induced in the receiving antenna? Is it possible to create WPT devices where radiation into the far zone is suppressed while the dynamic fields between the antennas effectively deliver power to the load? How to properly engineer the optimal regime of long-distance WPT between small antennas? To our knowledge, these questions have not been answered in the available literature. In spite of the great diversity of radio-frequency WPT systems, the comparative role of the radiative and nonradiative regimes is not properly elucidated. An important issue is the suppression of radiation in short-range systems of nonradiative WPT. Dynamic coupling between two loop antennas was recently considered in Ref. [13], where this issue was addressed, focusing on visualizations of the power flow in space. In that paper, it was found that it is possible to maximize the ratio of the delivered power to the power available from the source and at the same time minimize the radiated power by optimizing the load resistance for a fixed value of the internal resistance of the source.

In this paper, we find simple formulae for the optimal load impedance and the corresponding maximized power-transfer efficiency that are valid for arbitrary internal impedance of the source. We use these results to understand physical mechanisms of power delivery accounting for dynamic interactions, clarify the role of far fields, and find the optimal frequency range where the parasitic radiation into the far zone is effectively suppressed, while dynamic, far-zone fields strongly contribute to the power delivered to the source. In particular, we reveal a possibility of achieving high transfer efficiency, above 80%, at distances of approximately 5 times the antenna size at the optimal frequency in the hundred-megahertz range.

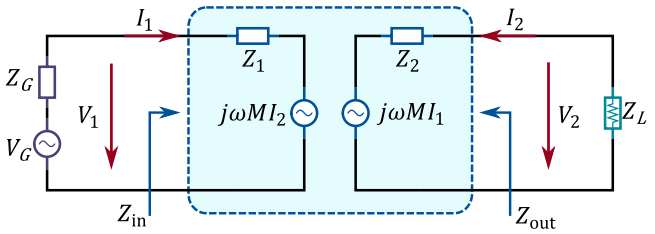

FIG. 1. Equivalent circuit model of the WPT system.

The developed theory of optimal load impedance and maximized power-transfer efficiency can be used for optimizing coupling between arbitrary antennas, including electric dipoles. However, we focus the study on loop antennas, because electric dipoles are used in WPT devices quite rarely [14–16], mainly in very short-range systems for high power transfer via capacitive coupling [17,18] and in WPT systems operating in lossy media, e.g., for biomedical implants [19]. Most WPT systems operating in free space utilize magnetic dipoles implemented as coils [1,2,20–22].

This study is also relevant for the understanding and use of nonradiating antennas—those creating only near fields, such as anapole antennas [23,24]. The evident advantage of anapole antennas is negligibly small parasitic radiation for all arrangements of the two antennas where mutual coupling of the antennas does not destroy the anapole properties. In Ref. [25], anapole antennas were claimed to be more beneficial for the short-range WPT than magnetic dipoles due to suppressed radiation. The use of the theory developed in this work allows us to understand full implications of radiation cancelation for power coupling between antennas.

The paper is organized as follows. In Sec. II, we theoretically analyze the dynamic coupling between two small WPT antennas, and elaborate the model of power-transfer efficiency (PTE) applicable for a maximally broad frequency range and maximal range of distances. In Sec. III, we study two key arrangements of TX and RX loops: coaxial and coplanar. Finally, the developed analysis is verified by full-wave simulations and experiments in Sec. IV.

II. WPT SYSTEM ANALYSIS

Figure 1 shows the equivalent circuit of WPT systems formed by two coupled antennas. The two antennas are represented by their individual input impedances Z_1 and Z_2. The transmitting antenna is fed by a voltage source V_G with internal impedance Z_G, and the receiving antenna is loaded by the load impedance $Z_L = R_L + jX_L$, whose real part R_L is the useful load.

Similarly to Ref. [13], we find it convenient to express the electromotive forces (EMFs) induced by antennas in one another through the complex coefficient $M = M_R +$

jM_I instead of the commonly used mutual impedance, generalizing the notion of mutual inductance to dynamic regimes, applicable to arbitrary distances between the antennas:

$$V_{\mathrm{emf},i} = j\omega M I_i. \tag{1}$$

Here, $i = 1, 2$ denote the first and second antennas. For inductive wireless power-transfer devices and in the quasistatic limit, M is real valued and equals the usual mutual inductance between the two coils. The value $Z_m = j\omega M$ is the mutual impedance, not to be confused with the induced impedances $Z_{11} = V_{\mathrm{emf},2}/I_1 = Z_m I_2/I_1$ and $Z_{22} = V_{\mathrm{emf},1}/I_2 = Z_m I_1/I_2$). For voltages $V_{1,2}$, we have

$$V_1 = Z_1 I_1 + j\omega M I_2 = V_G - I_1 Z_G, \tag{2}$$

$$V_2 = I_2 Z_L = -I_2 Z_2 + j\omega M I_1, \tag{3}$$

where $Z_{1,2} = R_{1,2} + jX_{1,2}$ are complex-valued antenna input impedances. The impedances seen from the source and the load (see Fig. 1) can be expressed in terms of the complex-valued mutual inductance M in the usual form:

$$Z_{\mathrm{in}} = \frac{V_1}{I_1} = Z_1 + \frac{\omega^2 M^2}{Z_2 + Z_L}, \tag{4}$$

$$Z_{\mathrm{out}} = \left.\frac{V_2}{I_2}\right|_{V_G=0} = Z_2 + \frac{\omega^2 M^2}{Z_1 + Z_G}. \tag{5}$$

Aiming for the maximal power coupling between antennas, we use the conventional definition of the PTE as the ratio of the power delivered to the load P_L and the power accepted by the input port of the transmitting antenna P_{in} (see, e.g., Ref. [2]):

$$\mathrm{PTE} \equiv \frac{P_L}{P_{\mathrm{in}}} = \frac{|I_2|^2 R_L}{\mathrm{Re}\{V_1 I_1^*\}}. \tag{6}$$

In this definition, the transfer efficiency does not depend on the internal impedance of the source Z_G, because the received power is normalized to the power accepted by the transmitting antenna. Using Eqs. (3) and (4), we write Eq. (6) in the form

$$\mathrm{PTE} = \frac{|I_2|^2 R_L}{|I_1|^2 \mathrm{Re}\{Z_{\mathrm{in}}\}} = \left|\frac{\omega M}{Z_2 + Z_L}\right|^2 \frac{R_L}{\mathrm{Re}\{Z_{\mathrm{in}}\}}. \tag{7}$$

The optimal load $Z_{L,\mathrm{opt}}$ maximizing the PTE can be found by nullifying the derivatives [26], i.e.,

$$\frac{\partial \mathrm{PTE}}{\partial X_L} = 0, \qquad \frac{\partial \mathrm{PTE}|_{X_{L,\mathrm{opt}}}}{\partial R_L} = 0, \tag{8}$$

from which we obtain the reactance and resistance of the optimal load that depends on the operational frequency and complex-valued mutual inductance:

$$X_{L,\mathrm{opt}} = -X_2 - \frac{\omega^2 M_R M_I}{R_1}, \tag{9}$$

$$R_{L,\mathrm{opt}} = \frac{\sqrt{R_1 R_2 - \omega^2 M_I^2}\sqrt{R_1 R_2 + \omega^2 M_R^2}}{R_1}. \tag{10}$$

This result generalizes expressions in Ref. [26], taking into account dynamic interactions between TX and RX antennas. Substituting Eqs. (9) and (10) into Eq. (7), the PTE of devices loaded by optimal loads after some algebra can be expressed in a very simple form:

$$\mathrm{PTE} = 1 - \frac{2}{1 + \sqrt{(R_1 R_2 + \omega^2 M_R^2)/(R_1 R_2 - \omega^2 M_I^2)}}. \tag{11}$$

Parameters M_R, M_I, R_1, R_2 can be found analytically, numerically, or experimentally.

The same expression for PTE can also be written in the form of the classical definition of impedance parameters, where $R_1 = r_{11}$, $R_2 = r_{22}$, $\omega M_I = r_{12}$, and $\omega M_R = x_{12}$ are the real and imaginary parts of the corresponding components of the impedance matrix of the wireless link:

$$\mathrm{PTE} = 1 - \frac{2}{1 + \sqrt{(r_{11} r_{22} + x_{12}^2)/(r_{11} r_{22} - r_{12}^2)}}. \tag{12}$$

In this form, this result can be used for optimization of power transfer between arbitrary emitters and receptors, not necessarily loop antennas.

The found simple analytical expression for the power-transfer efficiency at the optimal load allows us to perform a broadband analysis of the efficiency, find the optimal operational frequency, and clarify the role of radiation in short- and midrange WPT systems. Before moving to the analysis of systems with specific antennas, let us make some general observations. First, it is obvious that in order to increase the PTE we should increase the value of the square root in Eq. (11) or (12). Assuming that the two resistances are fixed, it is clearly beneficial to increase M_R, which, in the case of electrically small distances, simply means that the transfer efficiency is larger at smaller transfer distances. More interestingly, we see that increasing the imaginary part of M also leads to higher efficiency. The denominator under the square root cannot reach zero (which would mean 100% efficiency), because the mutual impedance cannot be higher than the impedance of both coupled circuits, but it can become rather small under some conditions. In the following, we discuss these two factors in an example of two coupled electrically small loops.

Since the power-transfer efficiency (6) and the optimal load impedance (9)–(10) do not depend on the internal impedance of the source Z_G, that can be chosen based on application requirements. It is also important to distinguish between the PTE and the system efficiency η_E that refers to the ratio of the power delivered to the load and the total input power from the power source [2]. If the WPT device should deliver the maximal power to the load, the source impedance can be conjugate matched to Z_{in}, in which case the source provides the maximum available input power. However, the system efficiency in this regime is limited by 50%. To maximize the system efficiency η_E, the internal resistance of the source Z_G is made as small as possible, to minimize dissipative losses. Thus, attempting to maximize η_E by matching the input impedance to the source impedance can cause the converter to reach its boundaries of the rated power. In this case, the converter losses can increase significantly, resulting in a high equivalent source impedance that is impractical for most WPT power sources. Importantly, our conclusions regarding optimization of PTE remain valid for any value of Z_G as long as the load impedance Z_L is equal to the optimal load given by Eqs. (9) and (10). If the load resistance is different, a matching circuit can be used at the receiver side. This approach and the ultrabroad range of possible operation frequencies is qualitatively different from that of Ref. [13], where the optimization was done for the case where $R_G \equiv \text{Re}\{Z_G\} = 50\ \Omega$, and the operation frequency range was specified in advance.

III. ANALYSIS OF A SYSTEM BASED ON LOOP ANTENNAS

Our goal is to clarify the role of intermediate and far fields in WPT systems in the maximally broad range of frequencies and for both short and middle ranges of distances, that is, when the distance between antennas can be comparable with the wavelength or electrically small. With this goal in mind, we restrict the size of both antennas so that in the whole possible operational frequency range the antennas remain electrically small. Otherwise, the comparison of the two regimes would be veiled by the size resonances of antennas.

In order to clarify the role of radiative fields, we consider small loop antennas and study WPT for coaxial and coplanar arrangements of the TX and RX antennas, as shown in Fig. 2. Because the loops are electrically small, we model them as magnetic dipoles (MDs). In the coaxial arrangement, the loops are coupled solely by near fields, since a magnetic dipole does not radiate along its magnetic moment. In this case, there is no radiative WPT, and the radiation resistances of the loops are purely parasitic contributions to resistances $R_{1,2}$. Thus, in order to increase PTE, it is desirable to realize a regime of suppressed radiation. In the coplanar arrangement, the situation is nearly opposite. In this case, the quasistatic mutual coupling is weak because the mutual inductance is small, and the radiative WPT can dominate already at midrange distances.

A. Analytical model

1. Coaxial arrangement

Let us consider two loops, TX and RX, with radii a and b, respectively, positioned in free space and distance d apart, as shown in Fig. 2(a). In the spherical coordinate system, the magnetic field components are (see, e.g., Ref. [27])

$$H_r = j\,\frac{ka^2 I_1 \cos\theta}{2d^2}\left[1+\frac{1}{jkd}\right]e^{-jkd}, \tag{13}$$

$$H_\theta = -\frac{(ka)^2 I_1 \sin\theta}{4d}\left[1+\frac{1}{jkd}-\frac{1}{(kd)^2}\right]e^{-jkd}. \tag{14}$$

Here $k=\omega/c$ is the wave number in free space. When $a,b \ll d$, we can approximate $H_z \approx \text{const}(x,y)$ in the area $z=d, x^2+y^2<b^2$, i.e., the z component of the magnetic field created by TX in the area of the RX loop is nearly equal to its r component at the receiving loop center:

$$H_z \approx H_r = j\,\frac{kA_T I_1}{2\pi d^2}\left[1+\frac{1}{jkd}\right]e^{-jkd} \tag{15}$$

with $A_T=\pi a^2$. From Eq. (15) and Faraday's law $V_{\text{emf},2} = -j\omega\mu_0\pi b^2 H_z$, we find the complex mutual inductance M defined by Eq. (1) as

$$M \equiv M_R + jM_I = \frac{j\,\mu_0 k A_T A_R}{2\pi d^2}\left[1+\frac{1}{jkd}\right]e^{-jkd}, \tag{16}$$

where $A_R=\pi b^2$ is the area of the RX loop. In the quasistatic limit $kd \ll 1$, Eq. (16) transits to the known mutual inductance of two coaxial loops, applicable when $d \gg \max(a,b)$ [28].

2. Coplanar arrangement

Now we consider two loops positioned in the same x-y plane, as shown in Fig. 2(b). If $a,b \ll d$, we can write

$$H_z \approx -\frac{k^2 A_T I_1}{4\pi d}\left[1+\frac{1}{jkd}-\frac{1}{(kd)^2}\right]e^{-jkd}. \tag{17}$$

Then we have

$$M \equiv M_R + jM_I = -\frac{\mu_0 k^2 A_T A_R}{4\pi d}\left[1+\frac{1}{jkd}-\frac{1}{(kd)^2}\right]e^{-jkd}. \tag{18}$$

In the low-frequency limit, this expression also transits to the known quasistatic mutual inductance, when $d \gg$

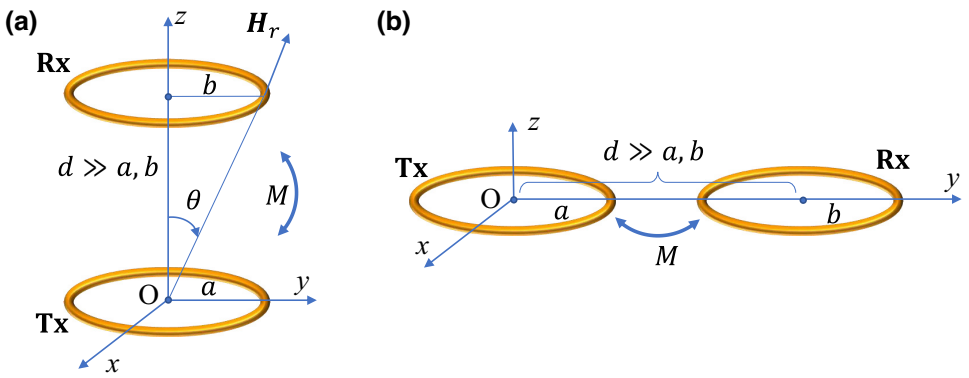

FIG. 2. Two magnetic dipoles in two case studies: (a) coaxial position; (b) coplanar position.

$\max(a, b)$ [28]. When $a = b$, the quasistatic approximation is applicable with high accuracy when $d > 4a$.

3. Input resistances of TX and RX loops

The input resistances R_1 and R_2 of the TX and RX antennas are the sums of the Ohmic resistances $R_{O1,O2}$ and radiation resistances $R_{r1,r2}$, i.e., $R_{1,2} = R_{r1,r2} + R_{O1,O2}$. For electrically small loops made of thin round wires in the regime of strong skin effect, we have (e.g., Ref. [27])

$$R_{O1} = \frac{a}{r_0}\sqrt{\frac{\omega\mu_0}{2\sigma_w}}, \qquad R_{O2} = \frac{b}{r_0}\sqrt{\frac{\omega\mu_0}{2\sigma_w}}. \tag{19}$$

$$R_{r1} = \eta\frac{\pi}{6}(ka)^4, \qquad R_{r2} = \eta\frac{\pi}{6}(kb)^4. \tag{20}$$

Here, r_0 is the radius of the antenna wire, σ_w is the conductivity of the wire, and $\eta = \sqrt{\mu_0/\varepsilon_0}$ is the free-space impedance. In numerical examples, we assume copper wires with $\sigma_w = 58.7 \times 10^6$ S/m, $a = b = 36$ mm, and $r_0 = 2$ mm.

Using Eqs. (16), (18), and (20), it is easy to verify that $\omega^2 M_I^2 \le R_{r1}R_{r2}$ for $d \ge \max(a, b)$ in both coaxial and coplanar cases, confirming that in Eq. (11) the expression under the square root is always positive.

B. Suppression of radiation of power into space

As discussed in Sec. I, it is important to clarify the role of radiation fields, since on the one hand, they create parasitic radiation of power into space, but on the other hand, far fields can carry power to the receiver. In this part, we consider this issue for coaxial loops.

Let us first discuss the case when the dissipation of energy in both transmitting and receiving coils can be neglected. Then, the quasistatic theory of wireless power transfer between two loops tells us that PTE = 1 identically, because the power accepted by the transmitting antenna can go only to the load in the receiver. However, it is expected that the fully dynamic model will show finite transfer efficiency even in the limit of zero distance between antennas, because the antennas will radiate some power into space. Thus, in Ref. [13] it was claimed that suppression of radiation into the far zone is a useful mean to increase power-transfer efficiency. Let us analyse this issue using the analytical formulae for the complex-valued mutual inductance and power-transfer efficiency. First, we note that in the absence of losses in coils, the resistances $R_{1,2}$ in Eq. (11) contain only radiation resistances of the two loops [see Eq. (20)]. On the other hand, the term ωM_I in Eq. (11) is the mutual resistance of the two antennas. It is obvious that, in the limit $d \to 0$, the mutual resistance becomes equal to the radiation resistance of the loops (for simplicity, we consider two identical loops), and PTE (11) tends to unity, although the radiation of energy from both loops is fully accounted for. Physically, this means that at small transfer distances, selection of the optimal load value given by Eqs. (9) and (10) leads to a WPT system with suppressed radiation into the far zone.

Perfect radiation suppression takes place only in the limit of zero distance, because the mutual resistance decays with increasing transfer distance. For the case of two coupled loops, this decay is illustrated in Fig. 3. We see that, for $d < 0.2\lambda$, the mutual resistance exceeds 80% of the radiation resistance. This means that if the currents in the loops have opposite phases, the dynamic interaction of the two loops will cancel at least 80% of the radiation into space, enhancing the received power. To show that the mutual coupling decreases the radiation, we derive the ratio between I_2 and I_1 for the case when $R_L = R_{L,\text{opt}}$ and $X_L = X_{L,\text{opt}}$, which reads

$$\frac{I_2}{I_1} = \frac{-R_1\omega(M_I + jM_R)}{R_1R_2 + j\omega^2 M_R M_I + \sqrt{(R_1R_2 - \omega^2 M_I^2)(R_1R_2 + \omega^2 M_R^2)}}. \tag{21}$$

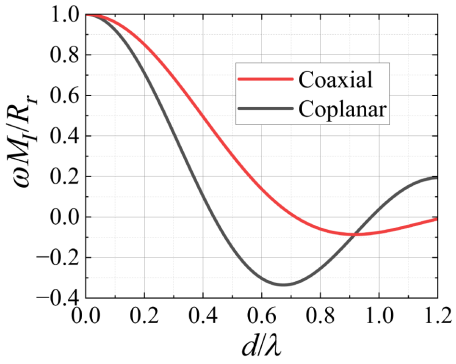

FIG. 3. Ratio of the mutual resistance to the radiation resistance for coaxial and coplanar arrangements of the TX and RX loops versus the normalized distance d/λ between the loop centers.

It can be observed from Eq. (21) that, when $R_1 = R_2 = \omega M_I$, the ratio between the currents indeed equals -1, which indicates that the currents have equal amplitudes and opposite phases (180°). Obviously, the magnetic dipole radiation of the set of two antennas is suppressed in this case. Next, we plot the ratio of the currents in the two loops, I_2/I_1, for both the amplitude and phase; see Figs. 4(a) and 4(b). We take as an example the case when the distance between the loops is 5 times larger than the loop radius, $d = 5a$. We see that at the optimal load (dashed curves) the regime of radiation suppression holds in the low-frequency range, since the currents in the two loops are approximately equal in amplitude and opposite in phase.

Thus, such a set of two antennas radiates into the far zone only via its higher-order multipoles. An estimation of the ratio between the radiated power from a single magnetic dipole and the power radiated from a quadrupole formed by two counterdirected dipoles of the same amplitude (both in the coaxial and coplanar arrangements) gives

$$\frac{P_q}{P_d} = \frac{1}{48\pi}(kd)^2, \tag{22}$$

which is approximately 6×10^{-4} for $kd = 0.5$. Thus, for the case of midrange WPT distances, this higher-order multipole radiation can be neglected.

Corresponding calculations for nonoptimal values of the load resistance (solid curves in Fig. 4) show that radiation is compensated in a certain frequency range but not in the low-frequency regime. However, the analysis of the PTE dependence [Fig. 4(c)] reveals that the efficiency remains practically unity in a broad frequency range, and also at low frequencies even for nonoptimal loads, which is due to the fact that radiation is in any case weak at low frequencies. The frequency of the sharp drop of efficiency at high frequencies corresponds approximately to the frequencies above the first null of the dependence of the mutual resistance on the frequency (Fig. 3). The value $d/\lambda = 0.5$ corresponds to approximately 8×10^8 Hz for the chosen example value of d. We conclude that if the dissipative losses in the loop antennas can be neglected, the radiation into the far zone is effectively suppressed due to dynamic antenna interactions up to the transfer distances of the order of one wavelength. Obviously, there is no need to use any special means to suppress parasitic radiation losses in this regime.

Let us next consider midrange interactions of loop antennas, taking onto account dissipation in the loops. Figure 5 shows the same plots as Fig. 4, but accounting for dissipative losses in both loops, as defined by Eq. (19). We see that in this case by selecting the optimal load impedance, we realize the regime of effective suppression of radiation, but only in a certain frequency range, approximately between 10^8 and 10^9 Hz. In this range, the currents in the two loops are approximately of the same amplitude

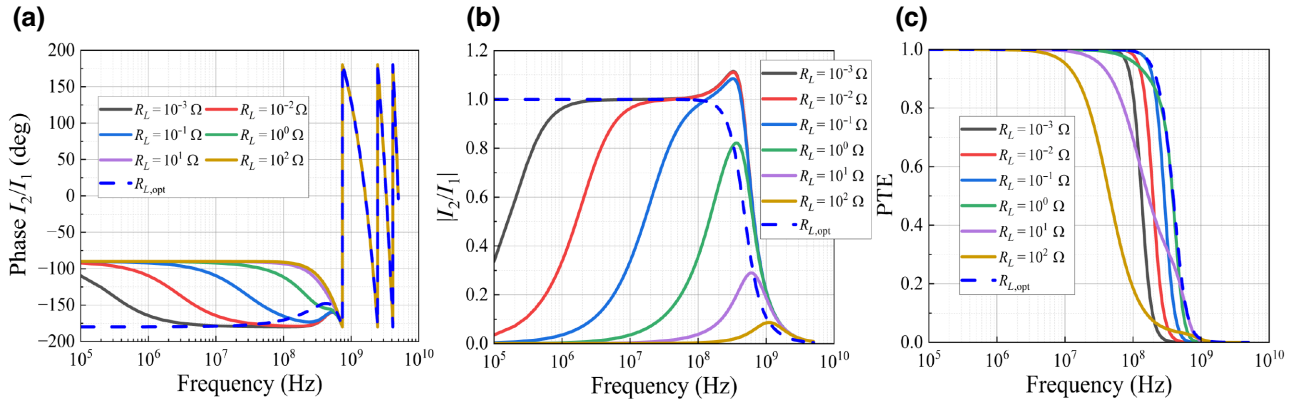

FIG. 4. Midrange coupling between two lossless loops: (a) phase difference between the loop currents; (b) magnitude of the current ratio I_2/I_1; (c) PTE for different values of the load resistance R_L. The dashed curves correspond to the optimal resistance, maximizing PTE.

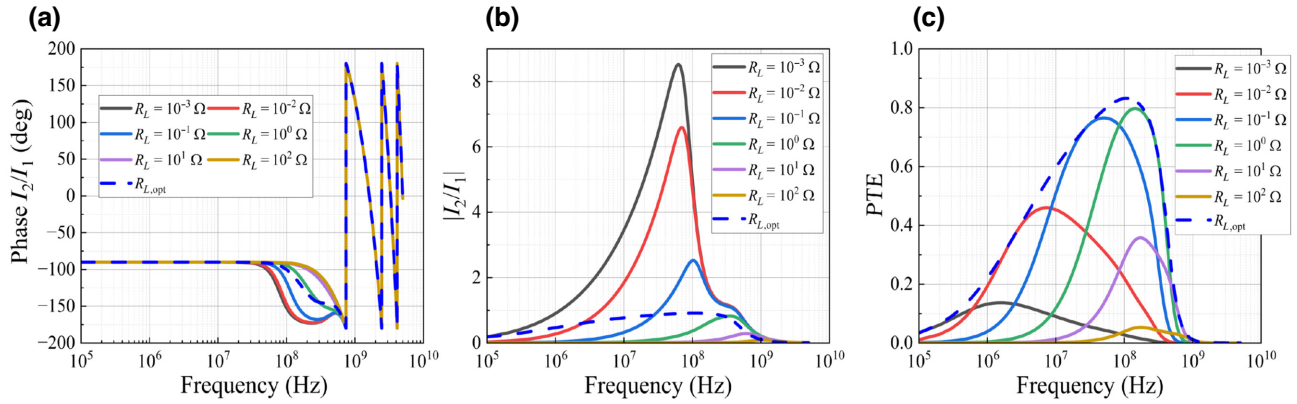

FIG. 5. Midrange coupling between two lossy loops: (a) phase difference between the loop currents; (b) magnitude of the current ratio I_2/I_1; (c) PTE for different values of the load resistance R_L. The dashed curves correspond to the optimal resistance, maximizing PTE.

and of opposite phase. At low frequencies, the phase difference between the currents is rather close to 90° for a broad range of load resistances (in all cases, the load reactance is the optimal one). This conclusion follows from Eq. (21) by setting the imaginary part of the mutual inductance M_I to zero.

To understand these effects, we need to consider the relative values of the Ohmic resistance and the radiation resistance, because the significance of radiation loss suppression is determined by the relative level of losses due to dissipation in the antennas and parasitic radiation into the far zone. To estimate this ratio, in Fig. 6 we plot all relevant resistances as functions of the frequency for the considered example of two loops.

We see that at low frequencies the loss resistance strongly dominates over the radiation resistance. For this reason, radiation suppression has a negligible effect on performance in the quasistatic regime. The power-transfer efficiency is low because the quasistatic coupling between loops at such large distances is weak. On the other hand,

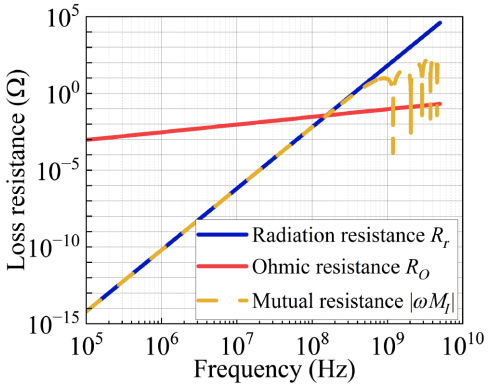

FIG. 6. Comparison of Ohmic resistance (19) and radiation resistances of one loop antenna (20), together with the mutual resistance between two antennas ωM_I. The loop radius $a =$ 36 mm, and $d = 5a$.

we observe that exactly in the frequency range of the radiation loss suppression for each considered value of the loss resistance, the power-transfer efficiency has a strong peak.

For electrically small transfer distances, the imaginary part of the mutual inductance M_I is negligibly small, and the general formula (11) tells us that higher efficiency corresponds to smaller distances d between the antennas (equivalently, to large values of the mutual inductance M_R). This holds for conventional inductive WPT devices. Now we see that at electrically larger distances between the two antennas there is another possibility to realize high-efficiency wireless power transfer. This regime takes place when M_I is large and the far-field radiation is suppressed. In this regime, we do not need high values of the real part of the mutual inductance. These results open a possibility to realize high-efficiency wireless power transfer to distances that are large compared to the antenna sizes.

The results may also have importance for nano-optics, namely, for the so-called Förster resonant energy transfer between a fluorescent donor molecule and an acceptor one (usually fluorescent at lower frequencies). Quantum electrodynamics (QED) allowed Salam [29] to prove that the matrix elements of the resonant energy exchange between two molecules can be correctly calculated using the model of their multipolar electromagnetic response. For two-level quantum systems, whose fluorescence and absorption spectra are Lorentzian, this means that their electromagnetic coupling should obey the laws of classical electrodynamics. However, the literature on the resonant intermolecular energy transfer prefers to use the QED theory methods. On the other hand, this literature utilizes a very simplistic treatment of the results obtained with the use of QED. If the donor-acceptor distance d is smaller than the so-called critical or Förster's distance d_F (this regime is called Förster resonant energy transfer), the energy transfer between molecules is claimed in this literature to be radiationless (see, e.g., Refs. [30–35]).

Papers treating Förster resonant energy transfer (FRET) start from the assertion that FRET is a radiationless process in which only virtual photons take part. In this literature, virtual photons suddenly disappear, being substituted with real photons when $d > d_F$. At these distances FRET transforms into radiative energy transfer (RET) [34], sometimes treated simply as resonant energy transfer [35]. In the theory of RET, quantum electrodynamics is used as well and explains why so many radiated photons are absorbed by a small acceptor located at a large distance [35].

To treat FRET as a radiation-free process and RET as a purely radiative process is a rough and potentially misleading approximation. In Ref. [30] it was correctly noted that d_F is the distance at which only one half of emitted photons are transferred to the acceptor, whereas another half are real photons radiated to free space. Indeed, for $d < d_F$, the virtual photons dominate (because the near field is larger than the wave field), but the real photons are emitted as well and this emission can be neglected compared to the virtual photon exchange only when $d \ll d_F$. Indeed, for $d > d_F$, the real photons dominate (because the wave field is larger than the near field), but the coupling by virtual photons is also present and becomes negligible only when $d \gg d_F$. The fact that a significant amount of radiated photons is absorbed by the small acceptor is the classical effect of resonant absorption (see, e.g., Ref. [36]). Briefly, we believe that the developed model of dynamic coupling between two dipoles and the found conditions for radiation suppression can be used as a classical electrodynamic model for a correct and simple description of both FRET and RET. In particular, we think that the present work points out the regime in which the RET efficiency may exceed 50%, because we see that the efficiency versus d does not drop monotonously and there is a revealed possibility of radiation suppression in short- and midrange coupling regimes.

C. Analytical results for optimized midrange WPT

Next, we study high-frequency midrange power transfer in more detail, considering various transfer distances and both coaxial and coplanar orientations of the loops. In our analysis, we focus on the almost radiation suppression regime in the midrange WPT, where the corresponding distance d is not very small compared to the wavelength but large compared to the loop radii a, b. In this case M_I is large in a rather broad range of frequencies, which helps to achieve high power-transfer efficiency.

In order to better clarify the roles of M_R and M_I in attaining the maximal PTE, we introduce two normalized coupling parameters $\kappa_R = \omega^2 M_R^2/R_1R_2$ and $\kappa_I = \omega^2 M_I^2/R_1R_2$, so that Eq. (11) takes the form

$$\mathrm{PTE} = 1 - \frac{2}{1 + \sqrt{(1+\kappa_R)/(1-\kappa_I)}}. \tag{23}$$

We fix the radii of the loops $a = b = 36$ mm and plot their values versus the normalized distance kd for many values of d from $d = 5a$ to $d = 50a$ and compare these coupling parameters with the similar plots of PTE. For each curve, the value of d is fixed, that is, the curves effectively show dependence on k (the frequency). The three corresponding plots are presented in Fig. 7 (coaxial arrangement) and Fig. 8 (coplanar arrangement).

We see that at $kd < 1$, at all midrange distances, PTE is low because the real part of the mutual inductance is large only in the near-field zone, when $d < a$, and also the imaginary part M_I is small compared to the Ohmic resistance. In other words, when $d \gg a$ and $kd < 1$, the loops are weakly coupled, leading to small values of PTE. In the conventional quasistatic regime of WPT, when $kd \ll 1$ and the antenna size a is comparable to the distance d, the mutual reactance $\omega M \approx \omega M_R$ is significantly larger than the Ohmic resistance. Therefore, in this conventional case of small distances and large loops we can achieve a high PTE according to Eqs. (11) and (23). Since the dipole-moment model of loops is not applicable in the quasistatic case, we study the quasistatic regime numerically and calculate the PTE in both coaxial and coplanar arrangements. The results are shown as dash-dot lines in Figs. 7(a) and 8(a), respectively. For very large electromagnetic distances where $kd \gg 1$, both coupling parameters and the PTE again exhibit low values. This is because the mutual impedance decreases in the far zone, whereas the radiation resistance of antennas rapidly grows versus frequency, i.e., versus kd. Thus, we can conclude that at midrange distances, where $kd \sim 1$, for any $d \gg a$, there is a range of optimal electrical distances kd corresponding to the maximal total coupling and, therefore, to the maximized PTE.

For the coaxial case, when there is no contribution of far fields to the power transfer, the decrease in the PTE at high frequencies is more rapid than its increase at low frequencies. For the coplanar case, the PTE curves are more symmetric, because at high frequencies not only does the radiation loss increase, but the far-field coupling also becomes stronger.

For the coaxial arrangement, the maxima of κ_R and κ_I as functions of kd occur at different values of kd. For example, for $d = 5a$, these maxima take place at $kd \approx 0.3$ and $kd \approx 0.5$, respectively. For $kd = 0.5$, we have, from Eqs. (16) and (20),

$$\omega M_I = \frac{\pi\eta k^2 a^4}{2d^2}\left(\frac{\sin kd}{kd} - \cos kd\right) \approx \frac{\pi\eta k^4 a^4}{6.15}, \tag{24}$$

which is close to $\pi\eta k^4 a^4/6 = R_{r1,r2}$. This shows that the radiation resistance of each of the two loops is almost compensated by the mutual resistance, and this case corresponds to the optimal nonradiative power transfer. Because of some residual radiation and the presence of losses

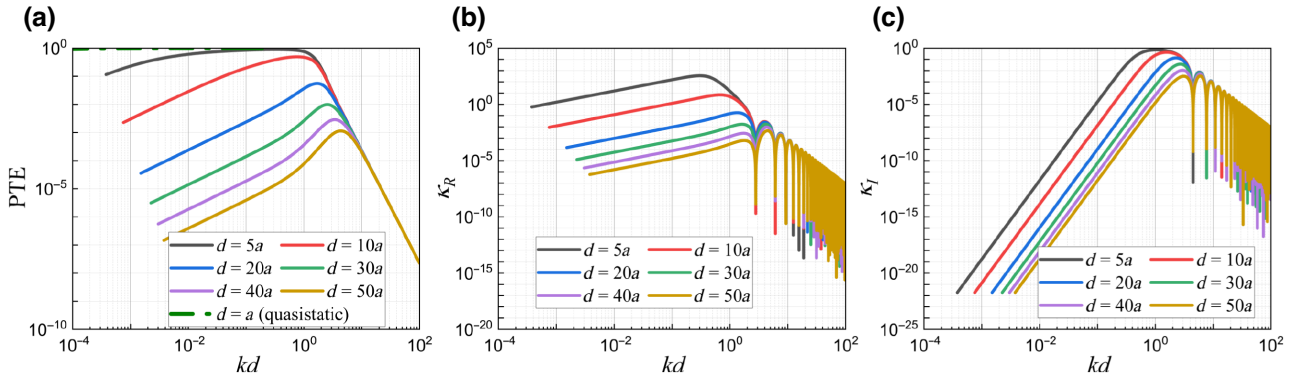

FIG. 7. Coaxial arrangement: (a) PTE versus kd; (b) κ_R versus kd; (c) κ_I versus kd for different values d/a from 5 to 50.

$\mathrm{PTE}|_{kd=0.5} \approx 0.89$, i.e., about 11% of the power is dissipated in resistors $R_{O1,O2}$ and radiated. However, the maximum of PTE (also about 0.9) holds not at $kd = 0.5$ but at $kd = 0.4$. At this point the sum $\kappa_R + \kappa_I = \omega^2|M|^2/R_1R_2$ is maximal. This regime can still be called the radiation-suppression regime because the maximum of function $\kappa_I(kd)$, as we can see in Fig. 7, is wide and overlaps with the maximum of $\kappa_R(kd)$, which is also wide, in accordance with Fig. 8. We note that, for our specific example, $kd = 0.4$ in the case $d = 5a$ corresponds to a frequency of 110 MHz. Below we see that this is the optimal WPT frequency for the considered example of two loops.

In the coplanar arrangement, maxima of $\kappa_R(kd)$ and $\kappa_I(kd)$ occur at $kd = 0.4$ and $kd = 0.8$, respectively, whereas $\kappa_R|_{kd=0.4} \approx 190$ and $\kappa_I|_{kd=0.8} \approx 0.7$. In this case the PTE also attains its maximum close to 0.7 at $kd = 0.6$ in the middle between the maxima of $\kappa_R(kd)$ and $\kappa_I(kd)$.

In the coaxial case, the far field plays a parasitic role, because the TX loop does not radiate into the RX direction. However, the important coupling parameter κ_I attains the maximum at a substantial electromagnetic distance ($kd > 1$) because the expression for M_I comprises two terms that compete with one another when kd is not very small and not very large. At still larger distances the efficiency quickly decays, since far-field coupling becomes small. For example, the maximal PTE at $d = 50a$ is as small as 0.001.

In the coplanar midrange ($1 < kd < 10$) case, the far field brings a contribution into both M_R and M_I, but also brings radiation loss measured by $R_{r1,r2}$. The optimal WPT is achieved for a substantial electromagnetic distance $kd \approx 5$ where κ_I is maximal and κ_R is close to the middle-range maximum. The far field plays an advantageous role at this distance, and the PTE in this optimal case is equal to 0.007. In other words, due to the contribution of radiation, the maximal PTE in the midrange region turns out to be 7 times higher than that obtained for the same large physical distance in the coaxial arrangement. In terms of the electromagnetic distance kd, the advantage granted by the far field is even higher because the optimal kd for the coplanar case ($kd = 5$) is larger than that for the coaxial case ($kd = 4$).

To conclude the discussion of Figs. 7 and 8, it is worth noting that in the far zone ($kd > \pi$) there are periodic maxima and minima of $\kappa_{R,I}(kd)$, whereas maxima of $\kappa_R(kd)$ coincide with the minima of $\kappa_I(kd)$ and vice versa (which results in a smooth decrease of PTE with the normalized distance kd). Two adjacent maxima (and

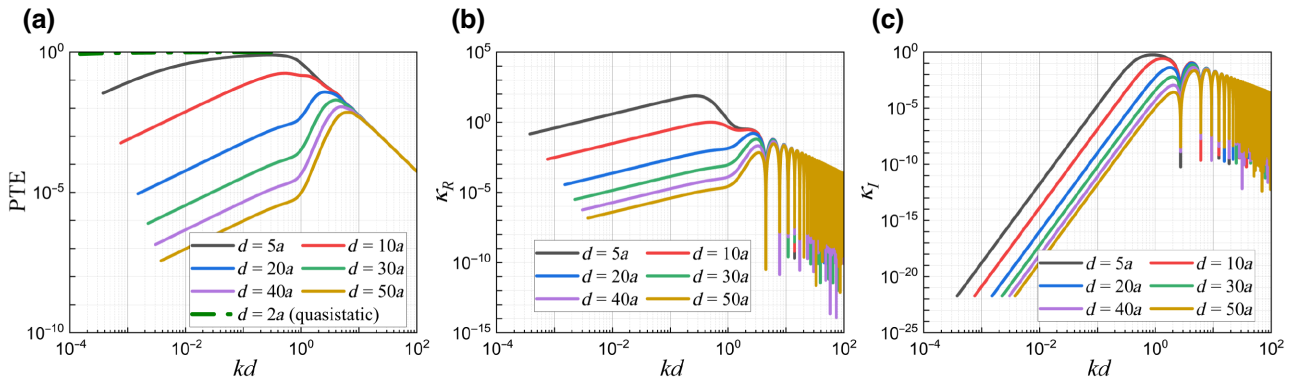

FIG. 8. Coplanar arrangement: (a) PTE versus kd; (b) κ_R versus kd; (c) κ_I versus kd for different values d/a from 5 to 50.

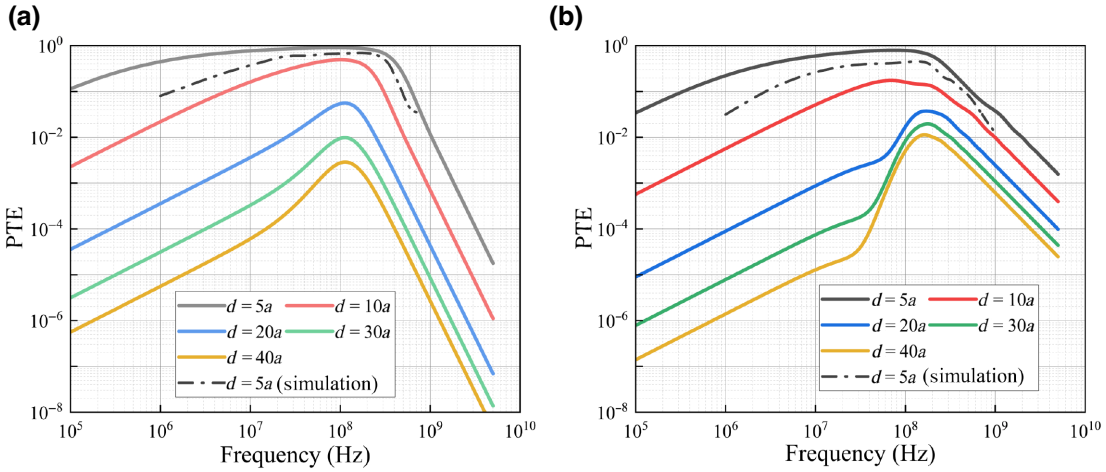

FIG. 9. PTE in a broad frequency range for different normalized transfer distances d/a: (a) coaxial arrangement; (b) coplanar arrangement.

minima) of κ_R (and κ_I) are distanced by 2π because the phase shift between the TX excitation and the field at the RX antenna position oscillates with period λ. At such large distances, we approach the far-field WPT regime, where one needs to use directive antennas instead of small dipole antennas.

Figure 9(a) shows PTE for the coaxial arrangement at frequencies from 500 kHz to 5 GHz with the normalized distance d/a changing from 5 ($d = 18$ cm) to 50 ($d = 1.8$ m). These results allow us to find the optimal operation frequency for practical long-distance (i.e., the transfer distance is much larger than the antenna sizes) WPT devices. Therefore, we perform a numerical validation of the model using a full-wave electromagnetic solver CST Studio together with the ADS simulation tool that models lossless matching circuits for the receiving loop at any frequency.

In Fig. 9(a), besides the analytical results (solid curves), we show the simulated PTE for $d = 5a$ (dash-dot curve). Qualitatively, this curve confirms the analytical model. Quantitative differences are as follows: the optimal operation frequency is 160 MHz instead of 110 MHz, and $\mathrm{PTE}_{\max} = 0.7$ instead of 0.9. The reasons for the disagreement are clear. In the analytical model, we replace the TX loop by a magnetic dipole, whereas in the simulations it is a split loop fed by a generator connected to a finite gap of width g. Therefore, besides a magnetic current mode, there is an electric dipole mode induced in the TX loop. The electric coupling of two loops also results in an electric dipole mode in the RX loop. Parasitic impact of electric coupling leads to a shift of the optimal frequency and makes cancelation of radiation less effective. At first glance, this parasitic effect can be made negligible by decreasing g; however, simulations show that $g \ll 1$ mm corresponds to a large split capacitance that completely shunts the loop, preventing its excitation.

In principle, it is possible to analytically optimize the loop even if the split is large. For such optimization, it is necessary to take into account the electric coupling of loops together with the magnetic one. However, this is not the purpose of this study. We aim to develop a theory that clearly explains the role of near and far fields in midrange WPT, which calls for the simplest possible analytical model to be used. Therefore, in simulations we simply numerically optimize the gap width g. The best correspondence of simulations and analytical theory holds when $g = 1$ mm and when the wire of the loop is slightly enlarged in the near vicinity of the split edges. Note that the problem of a finite gap exists only for the TX loop and does not arise for the RX loop. The electromagnetic solver allows us to load it by a lumped resistance whose value is determined by Eq. (10).

The corresponding numerical curve for the coaxial arrangement and $d = 5a$ is depicted in Fig. 9(a). In Fig. 9(b), we present a similar set of theoretical curves and the validation of the upper curve ($d = 5a$) for the coplanar arrangement.

Besides comparison of the analytical results with full-wave simulations, Figs. 9(a) and 9(b) lead to the following observations. First, we see that the optimal frequency of 110 MHz is the same for the coaxial arrangement at any considered d/a. The coincidence of these frequencies for the cases $d = 5a$ and $d = 50a$ has already been discussed above. Now, we observe it in the whole range d/a. Second, for the coplanar arrangement, as can be seen in Fig. 9(b), the absolute maximum of PTE shifts versus d/a. In accordance to the theory, it shifts from about 80 MHz ($d = 5a$, $\mathrm{PTE}_{\max} = 0.5$) to nearly 180 MHz ($d = 50a$, $\mathrm{PTE}_{\max} = 0.007$). Third, for both arrangements, the optimal frequency range is about 100–200 MHz, which is significantly lower than the self-resonance frequency of a wire loop with radius $a = 36$ mm. This frequency range results

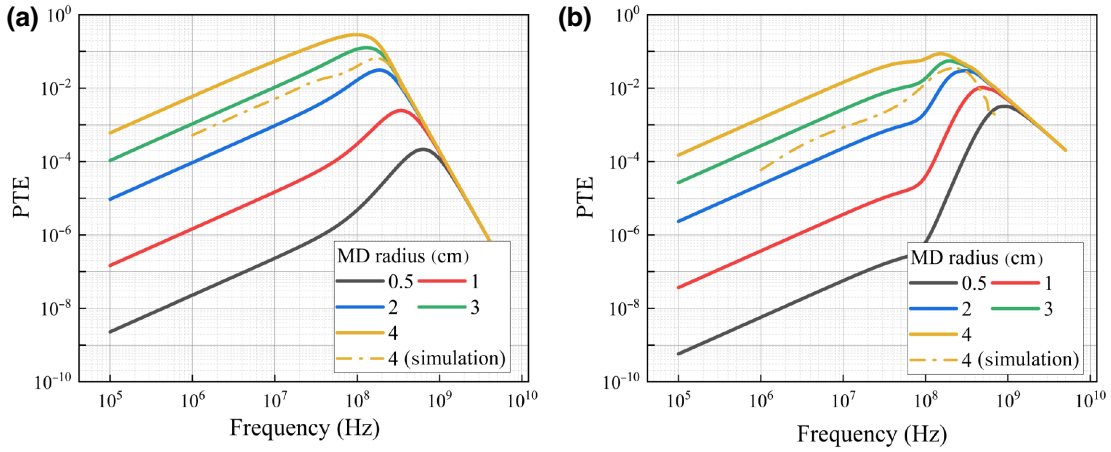

FIG. 10. PTE in a broad frequency range for different antenna sizes. The distance between the two antennas $d = 0.5$ m. (a) Coaxial arrangement; (b) coplanar arrangement.

from the formulae of the analytical model, confirmed by numerical simulations, and it is general: if a WPT device is based on two MDs, the maximal efficiency is achieved at a frequency much lower than the self-resonance of the individual antenna. However, this frequency is higher than those corresponding to the quasistatic regime—the regime in which $\omega M_I \ll R_{r1,r2}$.

In Ref. [37], numerical calculations similar to those presented in Fig. 9 were done for a different type of WPT. In Ref. [37], a spherical muscle phantom with a very small receiving antenna in the center was excited by a uniformly distributed source over the sphere surface. That ideal TX was creating a fixed incident electromagnetic power at all frequencies (reflections from the sphere boundary were assumed to be eliminated by an ideal antirefelecting coating). The RX antenna was assumed to be perfectly matched with the load and R_L was optimized for the maximal power transfer at every frequency. Full-wave simulations were performed in Ref. [37] with the aim of finding the optimal frequency of WPT for both electric and magnetic RX antennas. Interestingly, the set of curves plotted in Fig. 3 of Ref. [37] for different d/a qualitatively resembles our plots in both Figs. 9(a) and 9(b). The main qualitative difference is a negative shift of the optimal frequency versus d in Ref. [37]. This shift definitely results from electromagnetic energy dissipation in the medium. In the muscle tissue, the near-field coupling exponentially decays when d increases, and this decay factor is proportional to the frequency. Meanwhile, in the considered case two MDs are located in free space, and their near field at a given distance weakly depends on the frequency. However, the main qualitative result of the study [37] is the optimal frequency range for WPT located below the self-resonance of RX but higher than the low-frequency region in which the quasistatic approximation for the whole system is applicable. This result agrees with our result. In Ref. [38], the coupling of two MD-based antennas in a lossy medium is considered with the purpose of optimizing the antenna sizes for the given operating frequency. Again, the operation frequency turns out to be located between the low-frequency region and the band of the antenna self-resonance. And the same refers to the range of optimal operation frequencies when the TX and RX antennas are located in free space.

In Figs. 10(a) and 10(b), we present PTE versus frequency for both cases of coaxial and coplanar arrangements for a comparatively large fixed transfer distance $d = 0.5$ m and different loop radii a. We see that the optimal frequency decreases versus a. This decrease, evidently, results from the increase in the coupling for given frequency when the loop gets larger. The top theoretical curves in Figs. 10(a) and 10(b), i.e., the case $a = 4$ cm, are validated by numerical simulations. Again, we note a qualitative agreement, but the simulated $\mathrm{PTE}_{\max}$ is triply lower than the theoretical prediction for the coaxial arrangement and twice lower for the coplanar one. In other words, the numerical disagreement between the theory and simulations in the case $d = 12.5a$ is much larger than that in the case $d = 5a$, when the radiation suppression regime is achieved. This result confirms our insight that the main inaccuracy of the magnetic dipole model is not in the approximate formulae for the mutual inductance, but mostly in negligence of the electric dipole mode. For the loop $a = 4$ cm, this mode is more noticeable than for the loop $a = 3.6$ cm operating at the same frequency.

To conclude this section, let us formulate the most important theoretical observations.

(a) In the midrange coupling regime between two electrically small loops there is a possibility to reach reasonably high power-transfer efficiency due to suppression of radiation into the far zone (compensation of the radiation resistances of both loops), as presented in Figs. 7 and 8.

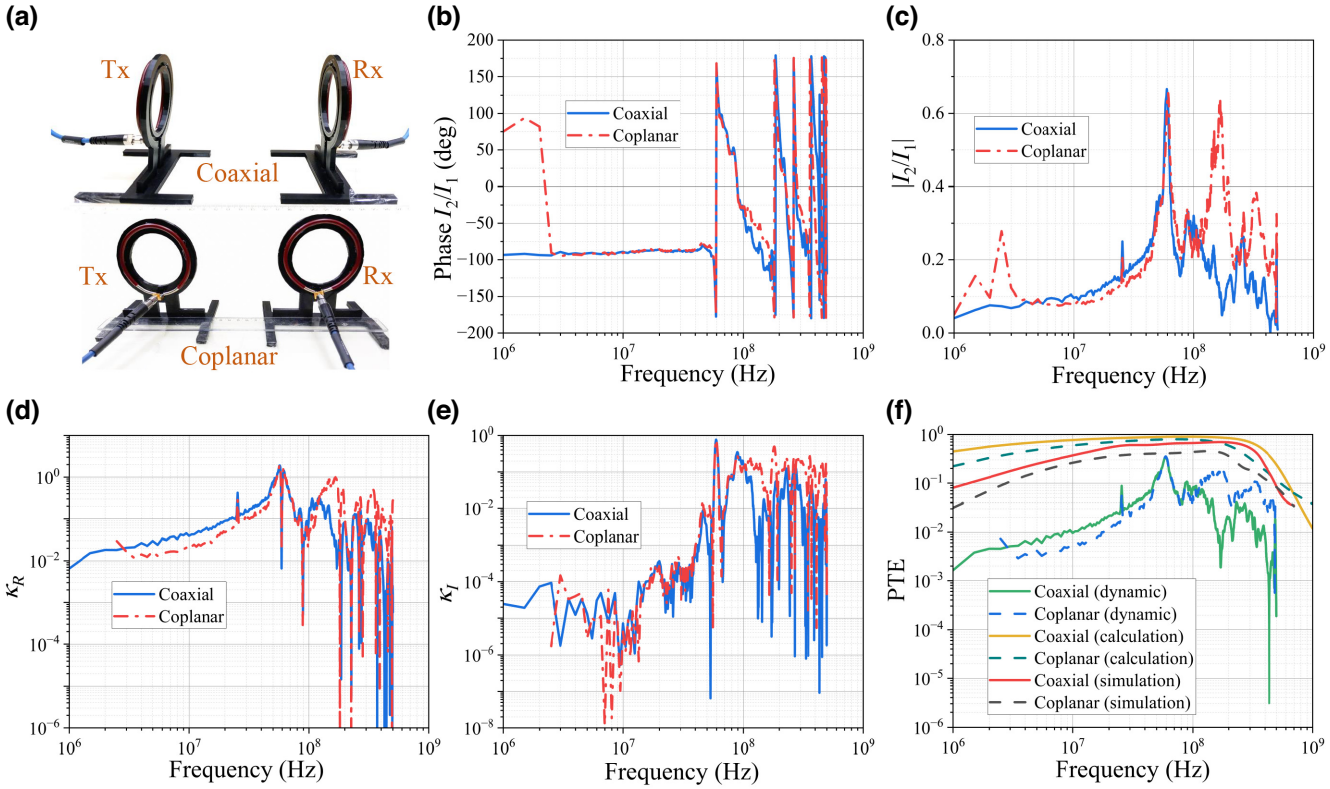

FIG. 11. Measurement setup and results: (a) two loop antennas in coaxial and coplanar arrangements; (b) phase difference of the loop currents; (c) magnitude ratio I_2/I_1; (d) κ_R; (e) κ_I; (f) PTE comparison between calculated, simulated, and measured results for coaxial and coplanar antenna arrangements.

(b) This regime is realized by tuning the load impedance to the optimal value for the maximal transfer efficiency [cf. Eqs. (9)–(11)]. Limitations of the optimal load matching are studied in detail in the Supplemental Material [39], which includes Refs. [27,40–43].

(c) The optimal frequency for WPT between two small loops to distances much larger than the loop sizes in both cases of the arrangement of TX and RX loops lies above the low-frequency region (in which the coupling of two antennas is quasistatic and strong) but below the resonance band of the individual loop antennas.

(d) To realize effective wireless power delivery at the maximally possible distance between small antennas, the midrange regime with the coplanar arrangement of loops is suitable. In this case, the far-field coupling grants a significant improvement of PTE compared to the case when WPT holds solely due to near fields, which makes the coplanar arrangement of loops advantageous compared to the coaxial one (as observed in Figs. 9 and 10).

IV. EXPERIMENTAL VERIFICATION

In this section, we present an experimental validation of the theoretical results. The experimental setup consists of two loop antennas designed for the frequency range of interest. In order to minimize the effect of the electric dipole mode, we use shielded loop antennas made from coaxial cables. The center conductor of the cables forms transmitting and receiving loops, and the cable screen serves as a shield, minimizing the electric dipole mode current. The two terminals of the inner copper wire of the loop are welded to the center pins and the ground parts of SMA connectors. The shield is cut close to the connection points. Both TX and RX loops have the same radius of 3.6 cm and are placed at a center-to-center distance of 18 cm ($d = 5a$) for coaxial and coplanar arrangements, as shown in Fig. 11(a). For each arrangement, the antennas are connected to two ports of the ZND vector network analyzer to measure Z parameters of the system in a wide frequency range, which allows evaluating the optimal frequency and PTE for the optimal load. The measured Z parameters are used for analytical calculations of the optimal load impedance and power-transfer efficiency using the formulae presented above. The experimental results are shown in Fig. 11.

We see that the phase difference and magnitude ratio I_2/I_1 of the currents in the transmitting and receiving loops show a qualitative agreement with numerical calculations (see the blue dashed lines in Fig. 5). At the optimal

frequency of 59.38 MHz for the coaxial and coplanar cases, the currents in the two loops have approximately opposite phases ($-177.451°, -175.341°$) and similar amplitudes (0.67, 0.607), as seen in Figs. 11(b) and 11(c). Here, the PTE has a peak (0.35/0.353) corresponding to the peak of κ_I, although κ_R is small, as seen in Figs. 11(d)–11(f).

Let us also compare PTE in the dynamic regime with the system working in the conventional quasistatic coupling regime. In this case, the loop coupling is defined by the mutual inductance, conventionally determined by the geometry and positions of the loops. To do that, we measure the mutual inductance and the Z parameters of the two coupled loops at distance $d = 5a$ and at a frequency of 4 MHz. The measured mutual inductance is approximately 0.56 nH for the coaxial case (around 0.508 nH in the numerical calculations) and 0.384 nH for the coplanar case (0.313 nH in the numerical calculations). Substituting the measured mutual inductances and measured resistances $R_{1,2} = \mathrm{Re}\{Z_{11,22}\}$ into Eq. (11), we find an estimation for the maximal achievable PTE at this distance of PTE $\approx$ 0.0065 for the coaxial arrangement and PTE $\approx$ 0.0035 for the coplanar arrangement. These values are dramatically smaller than those corresponding to the theoretical, simulated, and experimental curves shown in Fig. 11(f), confirming a possibility to significantly enhance power-transfer efficiency using properly tuned dynamic coupling.

Overall, we observe qualitative agreement between the theoretical and experimental results. Quantitative differences are a small shift in the optimal frequency range and an order of smaller magnitude of the PTE in the experiment compared to the numerical calculations. This big difference can be explained by losses in the dielectric support and in the galvanic contacts. Additionally, similarly to the simulations, the loop antennas used in the experiments consist of split loops with a finite gap. This deviation from the idealized analytical model introduces a parasitic impact of electric coupling. Furthermore, the presence of a slit in the loop creates a parasitic capacitance, resulting in a significantly lower self-resonance frequency as compared to the pure magnetic dipole. As a consequence, this leads to a shift in the optimal frequency and an increase of losses.

V. CONCLUSION

In this paper, we develop the dynamic theory of wireless power transfer between two antennas, specializing it for identical loop antennas. We consider WPT systems in free space to thoroughly investigate the radiation suppression regime based on analytical formulae available for antennas in free space. Generally speaking, WPT in free space is close to practical situations. The theory covers a very broad range of frequencies and refers to both short-range and midrange distances between the loops. Assuming that the RX antenna reactance is properly matched at every possible operational frequency and its useful load resistance is similarly optimized, we aim to find the optimal frequency range for a given loop size and track how and why the power-transfer efficiency changes with the distance. We study two most important mutual arrangements of the loops: the coaxial and the coplanar ones. In the first arrangement, the coupling between the TX and RX antennas is solely due to the near fields, in the second case the near-field coupling is low and the radiative, far-zone coupling exists. We show that, when the distance d is very small compared to the antenna size, and dissipation is negligible, the power-transfer efficiency can approach unity at whatever (low enough) operation frequency, and the only issue is proper matching of antennas. However, if d is larger than the loop diameter $2a$, finding the optimal operation frequency becomes crucial for WPT system design. For the coaxial arrangement, we find the optimal frequency that turns out to be unique for a broad range of distances ($5a \leq d \leq 50a$). For the coplanar arrangement, the optimal frequency depends on the distance, but this dependence is quite weak. In both cases, the optimal frequency lies below the self-resonance of the loop but above the band in which the quasistatic model is applicable for the WPT system. In this frequency range the interaction between the loops is dynamic, measured with both inductive and resistive parts of the mutual impedance.

The maximum value of the PTE turns out to be quite high in spite of the geometrically and electromagnetically substantial distance between the two antennas. In this optimal regime, the mutual coupling of two loops suppresses the radiation from the system, and almost all the power, which is not lost due to parasitic dissipation in the TX antenna, is transferred to the RX. We thoroughly study the prerequisites and peculiarities of this regime, which holds for both coaxial and coplanar arrangements, considering contributions and advantages of the near-field and far-field couplings for midrange distances. The developed analytical model is verified by full-wave simulations and is partially validated experimentally. We believe that the regime of the radiation suppression is very important not only because it grants high PTE for substantial transfer distances, but also because it prevents parasitic heating of the ambient around the WPT system. In reality, the effects of conventional foreign objects are usually not significant, as we typically do not place blocking conducting or magnetic objects in between the coils. The effect of foreign objects in the vicinity of the device will somewhat change the values of the impedance parameters, but the main effects of radiation compensation will remain in place. In this respect, it is noted that the revealed regime of radiation suppression in fact reduces interference with foreign objects as compared to conventional systems, due to the suppression of far fields.

Finally, our future research aims to further improve the experimental demonstration by incorporating the optimal

load on the receiver end and carefully measuring the power delivered to the load. Within the scope of this paper, we have placed emphasis on the concept of the developed dynamic theory and the identified radiation suppression regime in midrange WPT. We believe that these findings make a substantial contribution to the advancement of wireless power-transfer technologies and provide valuable insights for future research in this field.

ACKNOWLEDGMENTS

This work is partially supported by the Academy of Finland, project 338786, and the Academy of Finland postdoctoral researcher grant 333479.

[1] A. Kurs, A. Karalis, R. Moffatt, J. D. Joannopoulos, P. Fisher, and M. Soljačić, Wireless power transfer via strongly coupled magnetic resonances, Science **317**, 83 (2007).

[2] S. Y. R. Hui, W. Zhong, and C. K. Lee, A critical review of recent progress in mid-range wireless power transfer, IEEE Trans. Power Electron. **29**, 4500 (2014).

[3] W. Brown, The history of power transmission by radio waves, IEEE Trans. Microw. Theory Tech. **32**, 1230 (1984).

[4] J. Garnica, R. A. Chinga, and J. Lin, Wireless power transmission: from far field to near field, Proc. IEEE **101**, 1321 (2013).

[5] S. Li and C. C. Mi, Wireless power transfer for electric vehicle applications, IEEE J. Emerg. Sel. Top. Power Electron. **3**, 4 (2015).

[6] S. A. Al Mahmud, I. Panhwar, and P. Jayathurathnage, Large-area free-positioning wireless power transfer to movable receivers, IEEE Trans. Ind. Electron. **69**, 12807 (2022).

[7] W. M. Ng, C. Zhang, D. Lin, and S. R. Hui, Two-and three-dimensional omnidirectional wireless power transfer, IEEE Trans. Power Electron. **29**, 4470 (2014).

[8] N. Ha-Van, Y. Liu, P. Jayathurathnage, C. R. Simovski, and S. A. Tretyakov, Cylindrical transmitting coil for two-dimensional omnidirectional wireless power transfer, IEEE Trans. Ind. Electron. **69**, 10045 (2022).

[9] J. Feng, Q. Li, and F. Lee, Load detection and power flow control algorithm for an omnidirectional wireless power transfer system, IEEE Trans. Ind. Electron. **69**, 1422 (2021).

[10] K. Agarwal, R. Jegadeesan, Y.-X. Guo, and N. V. Thakor, Wireless power transfer strategies for implantable bioelectronics, IEEE Rev. Biomed. Eng. **10**, 136 (2017).

[11] I. A. Mashhadi, M. Pahlevani, S. Hor, H. Pahlevani, and E. Adib, A new wireless power-transfer circuit for retinal prosthesis, IEEE Trans. Power Electron. **34**, 6425 (2019).

[12] N. Ha-Van and C. Seo, Modeling and experimental validation of a butterfly-shaped wireless power transfer in biomedical implants, IEEE Access **7**, 107225 (2019).

[13] E. Shamonina, L. Solymar, and V. Kalinin, On wireless power transfer between coils in the presence of radiation, J. Phys. D **54**, 405502 (2021).

[14] Q. Chen, K. Ozawa, Q. Yuan, and K. Sawaya, Antenna characterization for wireless power-transmission system using near-field coupling, IEEE Antennas Propag. Mag. **54**, 108 (2012).

[15] J.-H. Kim, Y. Lim, and S. Nam, Efficiency bound of radiative wireless power transmission using practical antennas, IEEE Trans. Antennas Propag. **67**, 5750 (2019).

[16] T. Washiro, in *2021 IEEE Wireless Power Transfer Conference (WPTC)*, 2021, p. 1.

[17] X. Qu, H. Han, S. Wong, C. K. Tse, and W. Chen, Hybrid IPT topologies with constant current or constant voltage output for battery charging applications, IEEE Trans. Power Electron. **30**, 6329 (2015).

[18] M. T. Tran and W. Choi, Design and implementation of a constant current and constant voltage wireless charger operating at 6.78 MHz, IEEE Access **7**, 184254 (2019).

[19] A. N. Abdulfattah, C. C. Tsimenidis, B. Z. Al-Jewad, and A. Yakovlev, Performance analysis of MICS-based RF wireless power transfer system for implantable medical devices, IEEE Access **7**, 11775 (2019).

[20] Z. Huang, S. Wong, and C. K. Tse, An inductive-power-transfer converter with high efficiency throughout battery-charging process, IEEE Trans. Power Electron. **34**, 10245 (2019).

[21] Z. Zhang, F. Zhu, D. Xu, P. T. Krein, and H. Ma, An integrated inductive power transfer system design with a variable inductor for misalignment tolerance and battery charging applications, IEEE Trans. Power Electron. **35**, 11544 (2020).

[22] D. Wang, X. Qu, Y. Yao, and P. Yang, Hybrid inductive-power-transfer battery chargers for electric vehicle onboard charging with configurable charging profile, IEEE Trans. Intell. Transp. Syst. **22**, 592 (2021).

[23] A. E. Miroshnichenko, A. B. Evlyukhin, Y. F. Yu, R. M. Bakker, A. Chipouline, A. I. Kuznetsov, B. Luk'yanchuk, B. N. Chichkov, and Y. S. Kivshar, Nonradiating anapole modes in dielectric nanoparticles, Nat. Commun. **6**, 1 (2015).

[24] V. Savinov, N. Papasimakis, D. P. Tsai, and N. I. Zheludev, Optical anapoles, Commun. Phys. **2**, 1 (2019).

[25] E. Zanganeh, M. Song, A. C. Valero, A. S. Shalin, E. Nenasheva, A. Miroshnichenko, A. Evlyukhin, and P. Kapitanova, Nonradiating sources for efficient wireless power transfer, Nanophotonics **10**, 4399 (2021).

[26] P. Jayathurathnage, M. Vilathgamuwa, and C. Simovski, in *2018 IEEE 4th Southern Power Electronics Conference (SPEC)*, 2018, p. 1.

[27] C. A. Balanis, *Antenna Theory: Analysis and Design* (Wiley, Hoboken, NJ, 2005).

[28] W. Grover, *Inductance Calculations: Working Formulas and Tables* (D. Van Nostrand Company, Inc., New York, 1946).

[29] A. Salam, Resonant transfer of excitation between two molecules using Maxwell fields, J. Chem. Phys. **122**, 044113 (2005).

[30] D. L. Andrews, A unified theory of radiative and radiationless molecular energy transfer, Chem. Phys. **135**, 195 (1989).

[31] G. J. Daniels, R. D. Jenkins, D. S. Bradshaw, and D. L. Andrews, Resonance energy transfer: The unified theory revisited, J. Chem. Phys. **119**, 2264 (2003).
[32] S. K. Sekatskii and G. Dietler, Using magnetic dipole transitions for fluorescence resonance energy transfer, Anal. Biochem. **299**, 263 (2002).
[33] S. Zadran, S. Standley, K. Wong, E. Otiniano, A. Amighi, and M. Baudry, Fluorescence resonance energy transfer (FRET)-based biosensors: Visualizing cellular dynamics and bioenergetics, Appl. Microbiol. Biotechnol. **96**, 895 (2012).
[34] A. Periasamy, Fluorescence resonance energy transfer microscopy: A mini review, J. Biomed. Opt. **6**, 287 (2001).
[35] G. A. Jones and D. S. Bradshaw, Resonance energy transfer: from fundamental theory to recent applications, Front. Phys. **7**, 1 (2019).
[36] C. F. Bohren and D. R. Huffman, *Absorption and Scattering of Light by Small Particles* (Wiley, New York, 1983).
[37] I. Soares, M. Gao, A. Skrivernik, Z. Sipus, M. Zhadobov, R. Sauleau, and D. Nikolayev, in *2021 IEEE MTT-S Wireless Power Transfer Conference (WPTC 2021)* (2021), p. 1.
[38] S. Chu, C. Stevens, and E. Shamonina, Wireless power transfer in attenuating media, AIP Adv. **11**, 115303 (2021).
[39] See Supplemental Material at http://link.aps.org/supplemental/10.1103/PhysRevApplied.20.014044 for a detailed study of the limitations of matching.
[40] M. Liu, H. Zhang, Y. Shao, J. Song, and C. Ma, High-performance megahertz wireless power transfer: Topologies, modeling, and design, IEEE Ind. Electron. Mag. **15**, 28 (2021).
[41] A. L. F. Stein, P. A. Kyaw, and C. R. Sullivan, in *2017 IEEE Applied Power Electronics Conference and Exposition (APEC)*, 2017, p. 3723.
[42] Q. Deng, J. Liu, D. Czarkowski, M. K. Kazimierczuk, M. Bojarski, H. Zhou, and W. Hu, Frequency-dependent resistance of Litz-wire square solenoid coils and quality factor optimization for wireless power transfer, IEEE Trans. Ind. Electron. **63**, 2825 (2016).
[43] R. Bosshard, J. Mühlethaler, J. W. Kolar, and I. Stevanović, in *2013 Twenty-Eighth Annual IEEE Applied Power Electronics Conference and Exposition (APEC)* (2013), p. 1812.